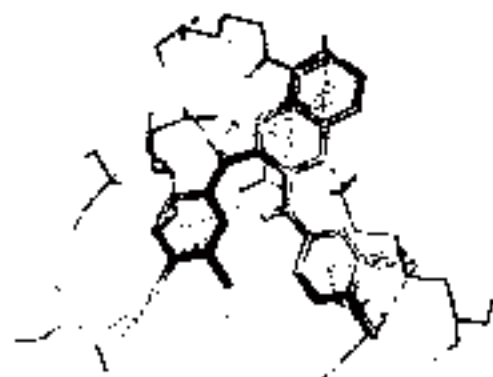
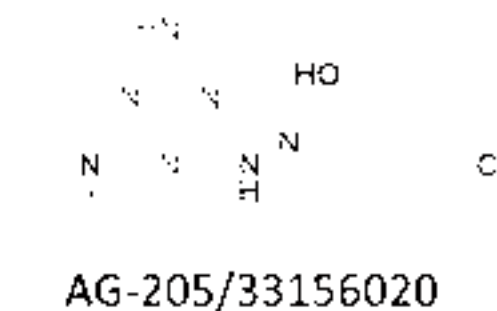


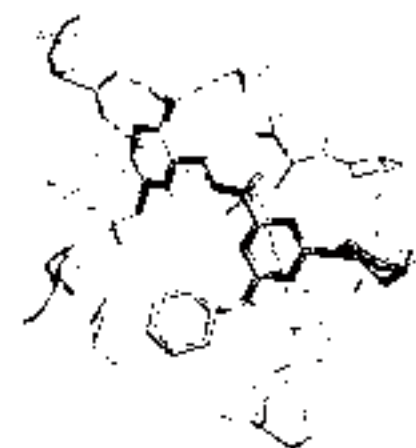
Drug
Screening



Target
Identification



MRSA MIC: 0.5 $\mu\text{g}/\text{mL}$
GyrB IC_{50} : 5.189 μM



MRSA MIC: 4-8 $\mu\text{g}/\text{mL}$
GyrB IC_{50} : 1.124 μM

Anti-MRSA Drug Discovery by Ligand-based Virtual Screening and Biological

Evaluation

Xu Lian^a, Zhonghua Xia^b, Xueyao Li^a, Pavel Karpov^{b,c}, Hongwei Jin^d, Igor V. Tetko^{b,c},

Jie Xia^{a*}, Song Wu^{a*}

^a*State Key Laboratory of Bioactive Substance and Function of Natural Medicines, Department of New Drug Research and Development, Institute of Materia Medica, Chinese Academy of Medical Sciences and Peking Union Medical College, Beijing 100050, China;* ^b*Institute of Structural Biology, Helmholtz Zentrum München-Research Center for Environmental Health (GmbH), Ingolstädter Landstraße 1, 85764 Neuherberg, Germany;* ^c*BIGCHEM GmbH, Valerystr. 49, 85716 Unterschleißheim, Germany;* ^d*State Key Laboratory of Natural and Biomimetic Drugs, School of Pharmaceutical Sciences, Peking University, Beijing 100191, China*

*Correspondence should be addressed to J.X. (jie.william.xia@hotmail.com) or S.W. (ws@imm.ac.cn)

Jie Xia & Song Wu

Institute of Materia Medica

Chinese Academy of Medical Sciences &

Peking Union Medical College

No. 2 Nanwei Road

Beijing 100050

China

Abstract

S. aureus resistant to methicillin (MRSA) is one of the most-concerned multidrug resistant bacteria, due to its role in life-threatening infections. There is an urgent need to develop new antibiotics against MRSA. In this study, we firstly compiled a data set of 2,3-diaminoquinoxalines by chemical synthesis and antibacterial screening against *S. aureus*, and then performed cheminformatics modeling and virtual screening. The compound with the Specs ID of **AG-205/33156020** was discovered as a new antibacterial agent, and was further identified as a Gyrase B (GyrB) inhibitor. In light of the common features, we hypothesized that the **6c** as the representative of 2,3-diaminoquinoxalines also inhibited GyrB and eventually proved it. Via molecular docking and molecular dynamics simulations, we identified binding modes of **AG-205/33156020** and **6c** to the ATPase domain of GyrB. Importantly, these GyrB inhibitors inhibited the MRSA strains and showed selectivity to HepG2 and HUVEC. Taken together, this research work provides an effective ligand-based computational workflow for scaffold hopping in anti-MRSA drug discovery, and discovers two new GyrB inhibitors that are worthy of further development.

Keywords: antibiotic resistance, MRSA, antibacterial agent, virtual screening, DNA Gyrase inhibitors

1. Introduction

The increasing emergence of antibiotic resistance poses a serious threat to public health worldwide [1]. Among the bacteria that developed antibiotic resistance, the ESKAPE pathogens, i.e., *E. faecium*, *S. aureus*, *K. pneumoniae*, *A. baumannii*, *P. aeruginosa* and *Enterobacter* species are the most important, as they are involved in many life-threatening infections and difficult to treat [2]. The ESKAPE pathogens resistant to clinically used antibiotics were covered by the World Health Organization (WHO) “priority pathogens” list for R&D of new antibiotics [3]. According to this list, *S. aureus* resistant to methicillin (MRSA) belongs to the class of “high-priority” pathogens.

MRSA is a major cause of both community and hospital-acquired infections such as complicated skin and skin structure infections, bacteremia, diabetic foot infection and community acquired pneumonia, and has led to remarkable increases in morbidity, mortality as well as overall healthcare costs [4]. At present, several drugs are available for the treatment of MRSA infections in clinic (e.g. vancomycin, daptomycin and linezolid). However, the safety concerns have limited their use in clinical practice [4]. Though new antibacterial agents with favorable toxicity profiles are in late clinical development phases, they are derived from previously approved drug classes and their mechanisms are the same [5]. To avoid cross-resistance, anti-MRSA agents with new chemotypes or new modes of action are urgently needed.

Virtual screening is a widely used strategy for hit identification [6], and has been proved fast and effective for discovery of new-chemotype antibacterial agents [7, 8]. As such, we applied this strategy to discover novel anti-MRSA agents. Unlike other studies that

completely used the known chemical structures with known activity as references for building ligand-based models [9-11], we newly compiled a set of compounds for cheminformatics modeling by chemical synthesis and bacterial growth inhibition assay. The chemical series that we focused on was the 2,3-diaminoquinoxaline (cf. Figure 1). Recently, several derivatives were reported as antibacterial agents against *S. aureus* RCMB010010 [12]. Due to the rather limited chemical data and the lack of knowledge on mode of action, however, no cheminformatics modeling work based on this chemical series had been done. Based on the data set, we built the common-feature pharmacophore models with six active 2,3-diaminoquinoxalines in the modeling set, and determined the optimal model by its performance evaluation with the actives and inactive 2,3-diaminoquinoxalines in the test set. Apart from this analysis, we also used the most potent derivative to generate a shape-based model and FCFP_6 fingerprints. By integrating the models into a computational workflow, we performed *in silico* and *in vitro* screening to identify diverse antibacterial agents against *S. aureus* with scaffolds different from the 2,3-diaminoquinoxalines. We also studied mode of action of the hit as well as the 2,3-diaminoquinoxalines, and proposed plausible binding modes by molecular docking and molecular dynamics simulations. In order to highlight the clinical significance of this research work, we presented the antibacterial activity against clinically-isolated MRSA and the cytotoxicity profile.

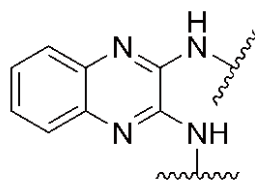


Figure 1. The 2,3-dianilinoquinoxaline scaffold in antibacterial agents against *S. aureus*

2. Results and Discussions

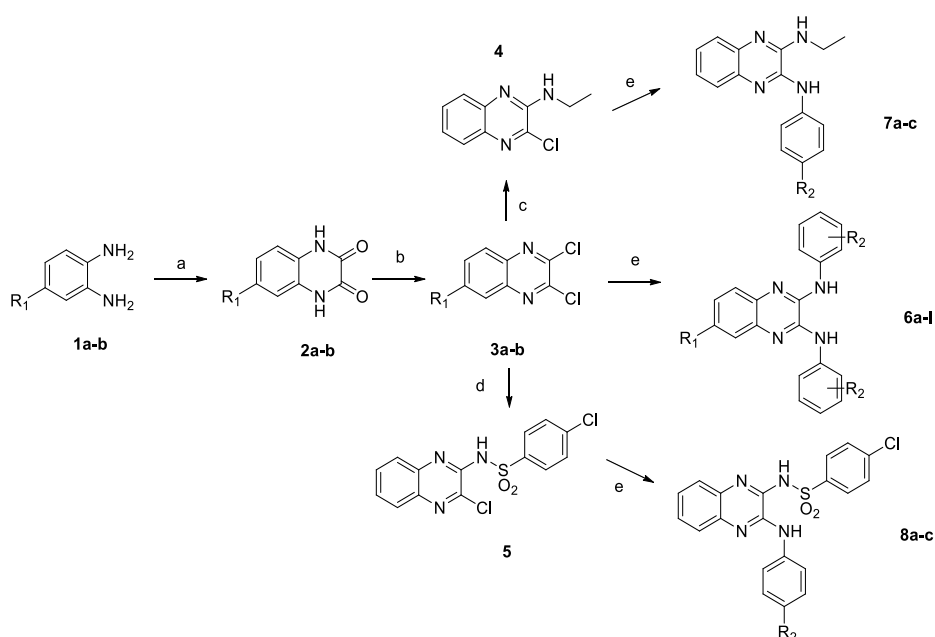
2.1 2,3-diaminoquinoxalines for computational modeling

Since pharmacophore modeling required a certain number of active and inactive compounds, we synthesized 18 derivatives with the 2,3-diaminoquinoxaline as the core scaffold and tested their antibacterial activity in term of MIC against *S. aureus* ATCC29213, a wild-type and methicillin-sensitive *S. aureus* (MSSA) strain, by the broth microdilution method [13].

The synthetic routes of the derivatives were designed and performed according to the previous publications [14-16], with minor modification. As shown in **Scheme 1**, the synthesis of **6a-f** started with the reaction between o-phenylenediamines (**1a-b**) and oxalic acid for the production of the 2,3-Quinoxalinediones (**2a-b**) [12]. By the chlorination of the 2,3-Quinoxalinediones and the substitution with various anilines to the 2,3-dichloroquinolines (**3a-b**), the target compounds were obtained. Notably, we used DMF as the solvent and aluminum trichloride as the catalyst in the last step, which led to a high reaction rate and a good yield (59%-80%). As for **7a-c**, the un-substituted 2,3-dichloroquinoline reacted with ethyl amine to produce the 3-chloro-N-ethylquinoxalin-2-amine (**4**), which was further substituted by different anilines at the position 3. The synthesis of **8a-c** was based on the same scheme as **7a-c**, except that 4-chlorobenzenesulfonamide was used to replace ethyl amine as the reagent in the reaction. All the target compounds were structurally validated by melting points, ¹H-NMR, ¹³C-NMR and HRMS.

The NH protons of **6a-f** revealed peaks in ¹H-NMR spectra at δ 9.15, 9.20, 9.37, 9.93, 9.81 and 8.96 ppm, respectively. The corresponding aromatic C-H protons of these

compounds were displayed in $^1\text{H-NMR}$ spectra as the signals from 7.20 to 8.32. As for compounds **6g-l**, the unique methyl groups on the quinoxalines can be identified in both $^1\text{H-NMR}$ and $^{13}\text{C-NMR}$ spectra. To be specific, their proton signals were respectively shown at δ 2.45, 2.45, 2.47, 2.43, 2.43 and 2.43 ppm in $^1\text{H-NMR}$, and their carbon signals were observed at δ 21.41, 21.41, 21.42, 21.40, 19.23, 21.40 ppm in $^{13}\text{C-NMR}$ spectra. With regard to compounds **7a-c**, the signals of two NH protons appeared at the positions different from those of compounds **6a-f** in the $^1\text{H-NMR}$ spectra. The two peaks were located at δ 8.77 ppm and 7.18 ppm for both **7a** and **7c**, and at 8.84 ppm and 7.21 ppm for **7b**. The other features of compounds **7a-c** included two signals of the ethyl groups in the $^{13}\text{C-NMR}$ spectra, i.e., δ 36.37 and 14.67 ppm for **7a**, δ 36.38 and 14.67 ppm for **7b**, and δ 36.38 and 14.66 ppm for **7c**. The structures of compounds **8a-c** were easy to validate from the $^1\text{H-NMR}$ spectra, according to the peaks at δ 12.36, 12.37, 12.33 ppm (for the NH protons of sulfonamide) and the signals at δ 9.10, 9.23, 8.93 ppm (for the NH protons of the phenylamino groups).



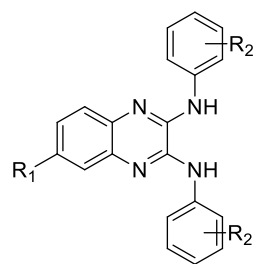
Scheme 1: The general synthetic route of the 2,3-diaminoquinoxalines. (a) 4N HCl, oxalic

acid, reflux, 4h; (b) SOCl₂, DMF; (c) Ethyl amine, EtOH, reflux, 8h; (d) 4-chlorobenzenesulfonamide, DMF, K₂CO₃, reflux, 4h; (e) R₂-PhNH₂, AlCl₃, DMF.

Their chemical structures and MICs are listed in Table 1. Although the structures of **6a**, **6b**, **6c**, **6e** and **6f** were previously reported, all of them were never tested against *S. aureus* ATCC29213 [12, 14, 17]. As shown in the table, **6a-l** showed potent antibacterial activity against *S. aureus* ATCC29213 (MICs: 0.1-3.13 µg/mL). **7a-c** could inhibit *S. aureus* ATCC29213 at the concentrations between 50 µg/mL and 100 µg/mL. However, **8a-c** were not active, with MICs greater than 100 µg/mL. The above data demonstrated a preliminary relationship between the chemical structures of 2,3-diaminoquinoxalines and the antibacterial activity for *S. aureus* ATCC29213. To be specific, (i) symmetrical substitutions of the 2,3-dichloroquinoxaline with the phenylamino groups were optimal for antibacterial activity (**6a-l** vs. **7a-c/8a-c**). When the phenylamino group on one side was replaced with either ethylamino- or sulfonamide- group, the antibacterial activity was significantly reduced. (ii) The electron-withdrawing substituents at the phenylamino group are better for antibacterial activity than the electron-donating groups, e.g. **6a-d** vs. **6e-f**, **6g-i** vs. **6k-l**. This set of compounds represents an ideal set of compounds for cheminformatics modeling.

Table 1: Chemical structures of the 2,3-diaminoquinoxalines and their antibacterial activity against *S. aureus* ATCC29213 in term of MIC (µg/mL).

Compound			<i>S. aureus</i>	
ID	R ₁	R ₂	ATCC29213(µg/mL)	Usage

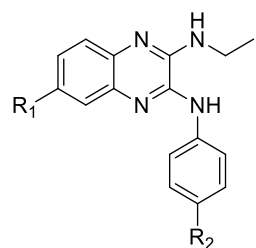


6a	H	4-Cl	0.2
6b	H	4-Br	0.2
6c	H	3,4-diCl	0.1
6d	H	3,4-diF	0.2
6e	H	4-Me	3.13
6f	H	4-Et	3.13

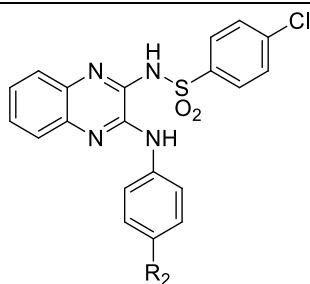
Modeling set

6g	CH ₃	4-Cl	0.39
6h	CH ₃	4-Br	0.2
6i	CH ₃	3,4-diCl	0.2
6j	CH ₃	4-Me	1.56
6k	CH ₃	4-Et	1.56
6l	CH ₃	4-Propyl	3.13

Test set



7a	H	4-F	100
7b	H	4-Cl	50
7c	H	4-Br	50



8a	H	4-F	>100
8b	H	3,4-F	>100
8c	H	4-Me	>100

2.2 *In silico* and *In vitro* screening for antibacterial agents

2.2.1 Computational models

We used Catalyst/HipHop module of Discovery Studio (v16.1.0, Dassault Systèmes Biovia Corp) to generate 10 common-feature pharmacophore models, based on six 2,3-diaminoquinoxalines with potent antibacterial activity against *S. aureus*, i.e. **6a-f**. The features of the pharmacophore models are shown in Table 2. The ranks of the pharmacophore models were very close, with 75.92 as the maximum and 73.26 as the minimum. The values of Direct Hit, Partial Hit and Max Hit were the same for 10 models.

Table 2. 10 common-feature pharmacophore models generated with the Catalyst/HipHop module in Discovery Studio.

Pharmacophore Model	Features ^a	Rank	Direct Hit ^b	Partial Hit ^c	Max Fit
pharm_01	XXZDH	75.92	111111	000000	5
pharm_02	XZZDH	74.75	111111	000000	5
pharm_03	XXZDA	74.72	111111	000000	5

pharm_04	RXZDH	74.46	111111	000000	5
pharm_05	XZZDA	73.55	111111	000000	5
pharm_06	XZZDH	73.43	111111	000000	5
pharm_07	XZZDH	73.35	111111	000000	5
pharm_08	XXZDH	73.34	111111	000000	5
pharm_09	XXZDH	73.31	111111	000000	5
pharm_10	RXZDA	73.26	111111	000000	5

^a X, hydrophobic from aromatic rings; Z, general hydrophobic; D, hydrogen bond donor; H, hydrogen bond acceptor lipid; A, hydrogen bond acceptor; R, ring aromatic. ^b Direct Hit: 1, a ligand fully matches the pharmacophore; 111111, all the ligands directly match the pharmacophore; ^c Partial Hit: 1, a ligand partially rather than fully matches the pharmacophore; 000000, no ligand partially matches the pharmacophore.

To facilitate model selection, the other 12 2,3-diaminoquinoxaline derivatives, i.e. **6g-l**, **7a-c** and **8a-c** were used as a test set for the evaluation of model performances in discriminating actives from inactives. According to Figure 2a, it is easy to identify **pharm_07** as the optimal model as it assigned the maximal values (4.7-5.0) to the actives whereas the minimal values (0.05-2.5) to the inactives. This model was composed of one hydrophobic feature for aromatic rings and two general hydrophobic features, one hydrogen bond donor, one hydrogen bond acceptor (cf. Figure 2b).

We used ROCS to build the shape-based model, with the lowest-energy conformer generated by Discovery Studio as the query. The model is shown in Figure 2c.

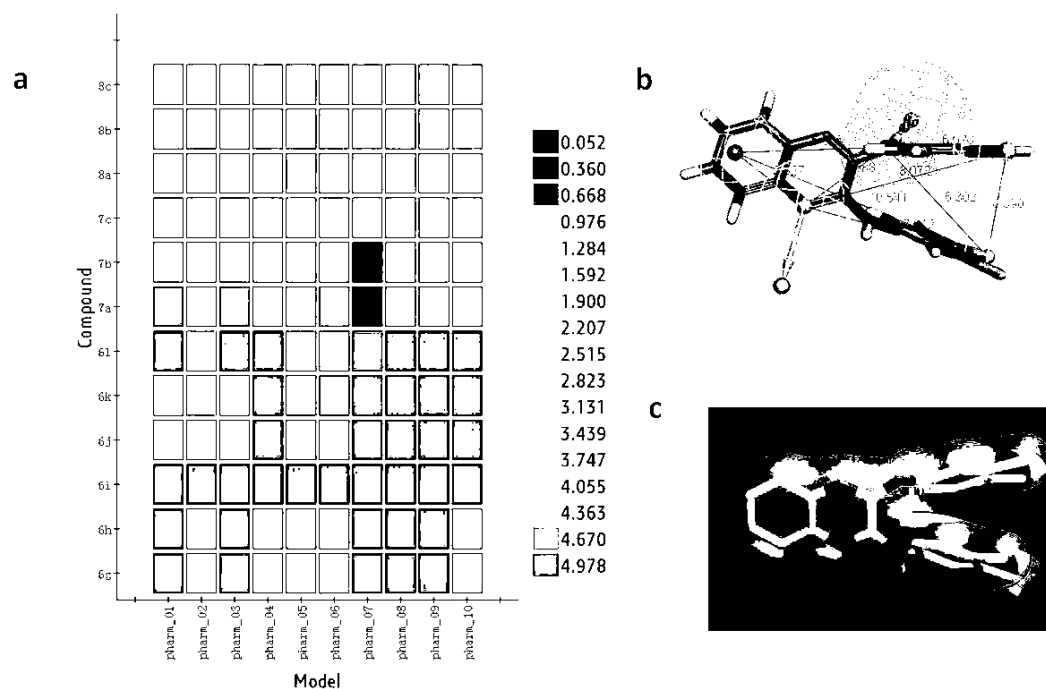
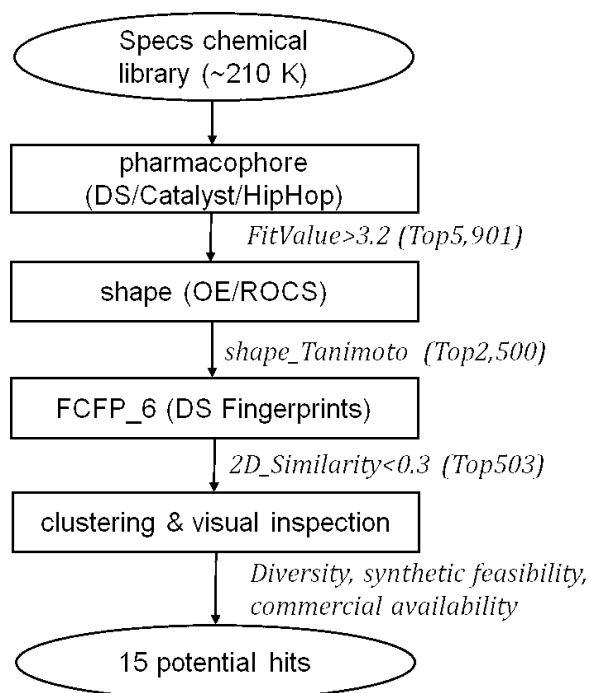


Figure 2. The models of the computational workflow. (a) The 2,3-diaminoquinoxalines in the test set are mapped to every pharmacophore model. (b) The optimal common-feature pharmacophore model. The model is composed of one hydrophobic feature from aromatic rings (blue) and two general hydrophobic features (light blue), one hydrogen bond donor (purple), one hydrogen bond acceptor (green). The most active 2,3-diaminoquinoxaline **6c** is mapped to the model. (c) The shape-based model from the lowest-energy conformation of **6c**.



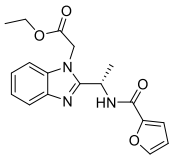
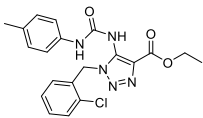
Scheme 2. The computational workflow for virtual screening.

2.2.2 Computational workflow

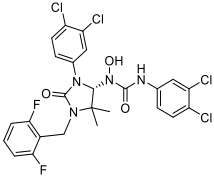
The computational workflow consisted of pharmacophore filtering, shape matching and fingerprints-based similarity search. We screened the Specs chemical library (~210,000 compounds) for potential antibacterial agents with the computational workflow. A total of 45,550 Specs compounds with their corresponding conformers/stereoisomers that matched **Pharm_07** passed the pharmacophore filtering. We only selected 5,901 compounds with the pharmacophore FitValues greater than 3.2. By matching the conformers to the shape-based models, we picked 2500 top-scoring compounds. Furthermore, we calculated 2D similarity in term of Tanimoto coefficient (Tc) between these compounds and compound **6c** based on FCFP-6 fingerprints. To identify hits with core scaffolds different from the 2,3-diaminoquinoxaline, we excluded the most similar compounds with the Tc values greater than 0.3 (i.e. 2,3-diaminoquinoxalines). From the other compounds with Tc values less than

0.3, we selected 503 compounds (Tc: 0.24-0.12). The structural clustering into 25 clusters based on FCFP_6 fingerprints facilitated the selection of structurally diverse compounds. By visual inspection, we selected one or two chemical structures from each cluster by giving priority to those with greater FitValues and shape Tc values, less fingerprint similarity as well as good synthetic feasibility. We selected 15 Specs compounds that were commercially available and had never been previously reported as antibacterial agents. The FitValues of these compounds ranged from 3.40 to 4.38, indicating of a relatively high pharmacophore similarity (Table 3). Their shape similarity values (Tc) were between 0.57 and 0.69, which demonstrated that they generally fit the shape of the most active derivative **6c**. Besides, the minimum of the fingerprint similarity (Tc) was 0.13, while the maximum was 0.22. It implied that the compounds somewhat shared common fingerprints with the most active derivative **6c** but also contained unique scaffolds.

Table 3. 15 potential hits selected from the computational workflow. The chemical structures, the similarity based on pharmacophore features, shape features and 2D fingerprints as well as their antibacterial activity (MIC) against *S. aureus* ATCC29213 are listed.

Specs ID	Structure	Similarity			<i>S. aureus</i> ATCC29213 ($\mu\text{g/mL}$) ^b
		Pharmacophore (FitValue)	Shape (Tc) ^a	Fingerprint (Tc)	
AT-057/43468612		3.40	0.68	0.14	>100
AO-476/41339614		4.38	0.61	0.14	>100

AS-710/43364291		3.50	0.69	0.13	>100
AG-205/40649626		3.58	0.58	0.13	>100
AO-081/41480557		3.96	0.58	0.18	>100
AK-968/41927008		3.90	0.60	0.17	>100
AE-641/40793067		4.08	0.61	0.15	>100
AG-205/33156020		3.72	0.62	0.16	6.25
AG-690/12245283		3.75	0.60	0.17	>100
AH-487/41801452		4.00	0.65	0.13	>100
AO-476/42169377		4.05	0.64	0.18	50
AG-690/11231009		4.03	0.65	0.22	>100
AN-584/43492661		4.00	0.57	0.19	>100
AP-064/41806449		3.93	0.64	0.14	>100

AG-690/08506044		4.22	0.59	0.16	>100
-----------------	---	------	------	------	------

^a: Tanimoto coefficient as a metric of structural similarity
^b: The assay was performed in duplicate and vancomycin was the positive drug (MIC: 1.56 µg/mL)

2.2.3 Experimentally validated hits

We purchased and tested 15 potential hits for their antibacterial activity against *S. aureus* ATCC29213. As shown in Table 3, the compound with the Specs ID of **AG-205/33156020** was experimentally validated as an antibacterial agent, and its MIC value was 6.25 µg/mL. Though not as potent as some of the 2,3-diaminoquinoxalines, it was structurally different from the 2,3-diaminoquinoxalines, with the fingerprint similarity (Tc) as low as 0.16. Figure S3 shows **AG-205/33156020** was well mapped to the pharmacophore model Pharm_07 (FitValue: 3.72). The successful identification of the diverse hit validated the effectiveness of our ligand-based computational workflow for scaffold hopping.

2.3 Mode of Action

2.3.1 Inhibition of *S. aureus* DNA Gyrase B

As mentioned above, **AG-205/33156020** was never tested against *S. aureus*. In order to understand its mode of action, we further analyzed the fragments of its chemical structure. It was interesting to see that this compound contained the fragment named arylaminotriazine, which appeared in the Gyrase inhibitors from Astrazeneca [18]. A few publications pointed out that Astrazeneca arylaminotriazines inhibited DNA supercoiling by targeting the ATP binding site of GyrB [19, 20]. With this evidence, we tested it for its inhibitory activity on GyrB. As a result, it showed moderate inhibition, with the IC₅₀ value of 1.1 ± 0.1 µM. Because its chemical structure well matched the optimal common-feature pharmacophore

model and the shape-based model derived from the 2,3-diaminoquinoxalines, we also tested the representative compound **6c** against GyrB. As expected, **6c** was a GyrB inhibitor, with an IC_{50} value of $5.2 \pm 0.1 \mu\text{M}$.

2.3.2 Plausible binding modes

The data above demonstrated that **AG-205/33156020** and **6c** were two new GyrB inhibitors with moderate antibacterial activity against *S. aureus*. With the crystal structure of GyrB (PDB code: 4URO), we performed molecular docking of the two compounds against GyrB with OEDocking module in OpenEye and then molecular dynamics (MD) simulations for 100 ns with AMBER 20 to further analyze the protein-ligand interactions. The RMSDs of the heavy atoms in GyrB and the two ligands as a function of time are shown in Figure 3b, where the protein structure or ligand structure in every frame is superimposed on the corresponding starting conformation by the CPPTRAJ program [21]. As for the system of GyrB in complex with **AG-205/33156020**, it reached equilibrium after about 40ns. The system of GyrB in complex with **6c** reached a plateau after approximately 80 ns. The respective protein-ligand binding mode after equilibrium was extracted and is shown in Figure 3c.

AG-205/33156020 binds to GyrB via forming (1) the hydrogen bonds between the phenolic hydroxyl group and Asp81/Gly85 as well as between the triazine fragment and His124, (2) the hydrophobic interactions with Pro87, Ala98, His124, Ile51, Ile86 and Ile175. **6c** binds at the entrance of the ATP binding site of GyrB. As expected, its 2,3-diaminoquinoxaline scaffold plays the most essential role in protein-ligand binding as it forms the electrostatic interaction with Arg84 and the hydrogen bonds with Lys118 and

Glu58. It should be noted that only one of the secondary amine groups interacts with the protein. Two dichlorophenyl groups interact with Thr173/Ile175 and Lys118/Ile102 via hydrophobic interactions, respectively. The details of the protein-ligand interactions from MD simulations may provide insights for further structural optimization.

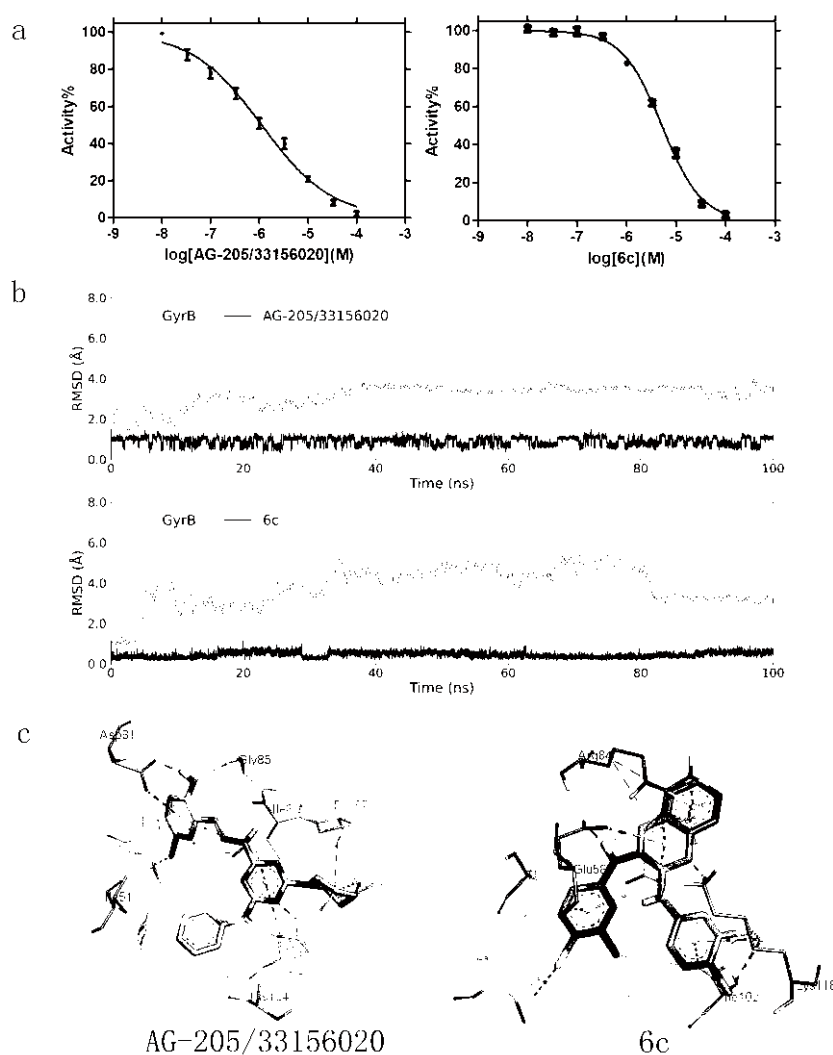


Figure 3. The molecular mechanism of compounds **AG-205/33156020** and **6c**. (a) The concentration-dependent ATPase inhibition of *S. aureus* Gyrase B (GyrB). The calculated IC_{50} values of **AG-205/33156020** and **6c** are $1.1 \pm 0.1 \mu\text{M}$ and $5.2 \pm 0.1 \mu\text{M}$, respectively. (b) Heavy-atom RMSDs of *S. aureus* GyrB and the ligands as a function of time during the 100-ns MD simulations. Each RMSD was calculated with the starting conformation/pose as

the reference. (c) Plausible binding modes of the two ligands to the ATP binding site of *S. aureus* GyrB as derived from MD simulations. Images were created with Discovery Studio 2016. The interacting residues and the ligands are shown in stick representations. Color codes: orange, residues; green, **AG-205/33156020**; purple, **6c**.

2.4 Anti-MRSA activity and cytotoxicity

To explore whether the two GyrB inhibitors were promising for further development, we tested their antibacterial activity against clinical isolates of MRSA by the broth microdilution assay [13], and their cytotoxicity to two mammalian cell lines by the sulforhodamine B (SRB) assay [22]. Table 4 lists the MIC values for three clinical isolates of MRSA. As shown in the table, both compounds can inhibit the growth of MRSA below the concentration of 10 $\mu\text{g/mL}$. Though not as potent as the last-resort antibiotics, i.e. vancomycin, **AG-205/33156020** achieved the MIC values of 4-8 $\mu\text{g/mL}$ (or 9.5-19.0 μM). **6c** was equivalent to vancomycin in term of potency, with the MIC value of 0.5 $\mu\text{g/mL}$ (or 1.1 μM). Regarding the cytotoxicity, the CC_{50} values of **AG-205/33156020** for human hepatocellular carcinoma (HepG2) cells and human umbilical vein endothelial cells (HUVEC) were 21 μM and 34 μM , while the values of **6c** were 4.9 μM and 10 μM , respectively. According to the above data, it is concluded that both hits showed anti-MRSA activity and were somewhat selective to HepG2 and HUVEC, but remained to be optimized.

Table 4. Antibacterial activity (MIC) and cytotoxicity (CC_{50}) of two newly-identified GyrB inhibitors

Compound ID	MIC ($\mu\text{g/mL}$)			CC_{50} (μM , mean \pm SD) ^a	
	MRSA 15-1	MRSA 15-2	MRSA 15-3	HepG2	HUVEC
AG-205/33156020	4	8	4	21 \pm 3	34 \pm 0.5
6c	0.5	0.5	0.5	4.9 \pm 0.4	10 \pm 2

vancomycin	0.5	1	1	n.d.	n.d.
------------	-----	---	---	------	------

^a values represent cytotoxicity after 72-hour treatment with the compounds. mean, the average of duplicate; SD, standard deviation.

3. Conclusion

MRSA has been defined by WHO as “high-priority” for new antibiotics discovery and development. This is somewhat attributed to cross-resistance, i.e. bacterial resistance to all the drugs of the same chemotype or mode of action. Discovery of novel antibacterial chemotypes may overcome this issue. In this study, we comprehensively employed chemical synthesis, cheminformatics analysis, ligand-based virtual screening and biological evaluation to identify novel anti-MRSA hits.

The 2,3-diaminoquinoxalines were previously reported as a new class of antibacterial agents against *S. aureus* [12], but the amount of the available derivatives was insufficient for cheminformatics modeling. To close the gap in experimental data, we first compiled a data set composed of 18 compounds with the 2,3-diaminoquinoxaline as the scaffold and with the MIC values ranging from 0.1 µg/mL to >100 µg/mL, by chemical synthesis and antibacterial screening against *S. aureus* ATCC29213. Based on the data set, we built 10 common-feature pharmacophore models with the DS/HipHop module and selected **pharm_07** out as the optimal model. We then integrated the pharmacophore model, the shape-based model and the FCFP-6 fingerprints of **6c** into the computational workflow, screened the Specs chemical library and identified a structurally different compound with moderate antibacterial activity against *S. aureus* ATCC29213, namely **AG-205/33156020**.

Furthermore, we performed bioassay to understand the mode of action and demonstrated that **AG-205/33156020** was a *S. aureus* GyrB inhibitor. Due to the same pharmacophore features and shape shared by **6c**, we hypothesized and eventually validated GyrB as one

protein target of **6c**. This is quite interesting as the protein targets of the 2,3-diaminoquinoxalines had never been reported before this study. By molecular docking and molecular dynamics simulations, we have proposed the most plausible binding modes of the two GyrB inhibitors, which would be helpful for hit-to-lead optimization. Further evaluation of anti-MRSA activity of the two new GyrB inhibitors and cytotoxicity to HepG2 and HUVEC has shown they effectively and somewhat selectively inhibit the growth of the MRSA strains. As no GyrB inhibitor was approved for clinical use after the withdrawing of novobiocin [23], both **AG-205/33156020** and **6c** may serve as good starting structures for development of new antibiotics.

4. Materials and Methods

4.1 Chemistry

4.1.1 General methods

All the reactions were monitored by thin layer chromatography (TLC) on the silica gel plates GF254 (0.20 mm, Yantai Chemical Industry Research Institute, China). High resolution mass spectrometry (HRMS) was performed by the LC/MSD TOF mass spectrometer system (Agilent Technologies Inc., USA). ¹H NMR spectra were all recorded on Bruker Avance III 500 spectrometer (Varian Mercury, USA) at the frequency of 500 MHz. ¹³C NMR (101 MHz or 126 MHz) spectra were recorded on Bruker 400 or 500 spectrometer. For the spectrometry, DMSO-*d*₆ was used as the solvent and tetramethylsilane was used as an internal standard. The column chromatography on silica gel (200-300 mm; Qingdao Haiyang Chemical Co., Ltd, China) was used for the purification of products. All the solvents and organic reagents were commercially available and not further purified.

4.1.2 General procedure for the synthesis of intermediates **2a-b**

The intermediates were prepared according to the synthetic routes proposed by El-Atawy M.A. et al.[12]. The o-phenylenediamine or 4-methylbenzene-1,2-diamine (**1a/1b**, 1 equiv) and anhydrous oxalic acid (1 equiv) were dissolved in 4N HCl (100 mL) in a round-bottom flask in a size of 250 mL. The mixture was refluxed at 100 °C for 4 h while being stirred. The reaction mixture was concentrated under reduced pressure. The residue was washed with ethanol (50 ml) and dried, which afforded 1,4-dihydroquinoxaline-2,3-dione (**2a/2b**) as white solid.

4.1.2.1 1,4-dihydroquinoxaline-2,3-dione (**2a**)

Yield 83%, white and powder-like solid. ¹H NMR (500MHz, DMSO-*d*₆) δ 11.93 (s, 2H), 7.12 (m, 4H). ¹³C NMR (126 MHz, DMSO-*d*₆) δ 155.79, 155.49, 132.73, 125.86, 124.20, 123.71, 115.60, 115.43, 20.98.

4.1.2.2 6-methyl-1,4-dihydroquinoxaline-2,3-dione (**2b**)

Yield 74%, white and powder-like solid. ¹H NMR (500MHz, DMSO-*d*₆) δ 11.85 (d, *J*=5.9 Hz, 2H), 7.01 (d, *J* = 8.2Hz, 1H), 6.92 (s, 1H), 6.87 (d, *J*=8.2Hz, 1H), 2.26 (s, 3H). ¹³C NMR (126 MHz, DMSO-*d*₆) δ 155.79, 155.49, 132.73, 125.86, 124.2, 123.71, 115.60, 115.43, 20.98.

4.1.3 General procedure for the synthesis of intermediates **3a-b**

The intermediates were prepared according to the reference [24]. The compounds **2a/2b** (1 equiv.) was placed in a round-bottom flask in a size of 250 mL and then SOCl₂ (10 equiv.) was added. The reaction mixture was stirred at 70°C for 4 h, followed by the concentration under reduced pressure. The residue was washed with n-hexane (50 mL) and then dried,

which afforded 2,3-dichloroquinoxaline (**3a/3b**) as a pale yellow solid.

4.1.3.1 2,3-dichloroquinoxaline (**3a**)

Yield 90%, pale-yellow solid. ¹H NMR (500MHz, DMSO-*d*₆) δ 8.13 (m, 2H), 8.00 (dd, *J*=21.0, 10.7 Hz, 2H). ¹³C NMR (126 MHz, DMSO-*d*₆) δ 145.08, 140.50, 132.25, 128.39, 123.44, 115.58.

4.1.3.2 2,3-dichloro-6-methylquinoxaline (**3b**)

Yield 77%, pale-yellow solid. ¹H NMR (500MHz, DMSO-*d*₆) δ 7.98 (t, *J*=7.0 Hz, 1H), 7.87(d, *J*=6.1 Hz, 1H), 7.80 (d, *J*=8.5Hz, 1H), 2.59 (s,3H). ¹³C NMR (126 MHz, DMSO-*d*₆) δ 144.86, 143.97, 142.91, 140.58, 138.95, 134.30, 127.8, 127.12, 21.76.

4.1.4 General procedure for the synthesis of target compounds **6a-l**

The synthesis of **6a-l** were performed according to the earlier publication [14]. A suspension of compounds **3a-b** (1 equiv.), aromatic amine (1 equiv.) and AlCl₃ (1.1 equiv.) in DMF (50 mL) was stirred at 110° C for 8 h. The reaction was quenched by cold water (50 mL). The product was extracted with ethyl acetate (3 x 75 mL). The organic phase was washed with water (2×20 mL) and brine (30 mL), dried with anhydrous Na₂SO₄. The solvent was evaporated under reduced pressure and then the solid was purified by flash column chromatography with petroleum ether/ethyl acetate (25:1) as the eluent.

4.1.4.1 *N*²,*N*³-bis(4-chlorophenyl)quinoxaline-2,3-diamine (**6a**)

Yield 71%, light yellow solid. m.p.: 236-239 °C. ¹H NMR (500 MHz, DMSO-*d*₆) δ 9.15 (s, 2H), 7.96 (d, *J* = 8.6 Hz, 4H), 7.60 (dd, *J* = 6.1, 3.5 Hz, 2H), 7.48 (d, *J* = 8.6 Hz, 4H), 7.40 (dd, *J* = 6.2, 3.5 Hz, 2H). ¹³C NMR (101 MHz, DMSO-*d*₆) δ 141.52, 139.67, 136.57, 128.97, 126.47, 125.98, 122.40. HRMS calcd for C₂₀H₁₄C₁₂N₄ [M+H]⁺, 381.0666; found, 381.0668

4.1.4.2 *N*²,*N*³-bis(4-bromophenyl)quinoxaline-2,3-diamine (**6b**)

Yield 74%, light yellow solid. m.p.: 253-255 °C. ¹H NMR (500 MHz, DMSO-*d*₆) δ 9.20 (s, 2H), 7.92 (d, *J* = 8.2 Hz, 4H), 7.60 (d, *J* = 8.6 Hz, 6H), 7.43 – 7.37 (m, 2H). ¹³C NMR (101MHz, DMSO-*d*₆) δ 141.50, 140.11, 136.55, 131.86, 126.01, 125.98, 122.79, 114.43. HRMS calcd for C₂₀H₁₄Br₂N₄ [M+H]⁺, 468.9658; found, 468.9623

4.1.4.3 *N*²,*N*³-bis(3,4-dichlorophenyl)quinoxaline-2,3-diamine (**6c**)

Yield 74%, yellow-green solid. m.p.: 151-153 °C. ¹H NMR (400 MHz, DMSO-*d*₆) δ 9.37 (s, 2H), 8.31 (d, *J* = 2.5 Hz, 2H), 7.89 (dd, *J* = 8.8, 2.6 Hz, 2H), 7.68 – 7.58 (m, 4H), 7.44 (dd, *J* = 6.2, 3.5 Hz, 2H). ¹³C NMR(101 MHz, DMSO-*d*₆) δ 141.35, 140.95, 136.48, 131.26, 130.94, 126.55, 126.16, 124.04, 121.62, 120.61. HRMS calcd for C₂₀H₁₂N₄Cl₄ [M+H]⁺, 448.9889; found, 448.9883

4.1.4.4 *N*²,*N*³-bis(3,4-difluorophenyl)quinoxaline-2,3-diamine (**6d**)

Yield 63%, yellow-green solid. m.p.: 216-218 °C. ¹H NMR (500 MHz, DMSO-*d*₆) δ 9.93 (s, 2H), 8.32 (d, *J* = 7.6 Hz, 1H), 8.29 (d, *J* = 7.2 Hz, 1H), 7.84 – 7.78 (m, 2H), 7.63 (dt, *J* = 6.6, 3.4 Hz, 2H), 7.49 (d, *J* = 9.6 Hz, 1H), 7.46 (d, *J* = 9.6 Hz, 1H), 7.41 (dd, *J* = 6.3, 3.5 Hz, 2H). ¹³C NMR (126 MHz, DMSO) δ 141.35, 137.92, 135.65, 126.11, 125.53, 123.47, 117.67, 117.30, 115.60, 109.70. HRMS calcd for C₂₀H₁₂N₄F₄ [M+H]⁺, 385.1071; found, 385.1064

4.1.4.5 *N*²,*N*³-di-*p*-tolylquinoxaline-2,3-diamine (**6e**)

Yield 73%, light yellow solid. m.p.: 146-148 °C. ¹H NMR (500 MHz, DMSO-*d*₆) δ 9.81 (s, 2H), 7.77 (d, *J* = 7.9 Hz, 4H), 7.52 (dt, *J* = 6.2, 3.3 Hz, 2H), 7.29 (dd, *J* = 6.3, 3.4 Hz, 2H), 7.20 (d, *J* = 7.8 Hz, 4H), 2.30 (s, 6H). ¹³C NMR (101MHz, DMSO-*d*₆) δ 141.73, 137.48, 132.81, 129.67, 125.62, 121.75, 21.03. HRMS calcd for C₂₂H₂₀ N₄ [M-H]⁻, 339.1615; found: 339.1605

4.1.4.6 *N*²,*N*³-bis(4-ethylphenyl)quinoxaline-2,3-diamine (**6f**)

Yield 58%, light yellow solid. m.p.: 127-130 °C. ¹H NMR (500 MHz, DMSO-*d*₆) δ 8.96 (s, 1H), 7.82 (d, *J* = 8.2 Hz, 2H), 7.54 (dd, *J* = 6.2, 3.5 Hz, 1H), 7.34 (dd, *J* = 6.1, 3.6 Hz, 1H), 7.27 (d, *J* = 8.1 Hz, 2H), 2.64 (q, *J* = 7.6 Hz, 2H), 1.25 (t, *J* = 7.6 Hz, 3H). ¹³C NMR (101 MHz, DMSO-*d*₆) δ 141.67, 138.53, 138.27, 136.66, 128.32, 125.73, 125.38, 121.26, 28.14, 16.24. HRMS calcd for C₂₄H₂₄N₄ [M+H]⁺, 369.2074; found, 369.2069

4.1.4.7 *N*²,*N*³-bis(4-chlorophenyl)-6-methylquinoxaline-2,3-diamine (**6g**)

Yield 62%, yellow-green solid. m.p.: 228-231 °C. ¹H NMR (500 MHz, DMSO-*d*₆) δ 9.42 (s, 2H), 8.01 (t, *J* = 9.1 Hz, 4H), 7.50 (d, *J* = 8.2 Hz, 1H), 7.46 (dd, *J* = 9.1, 2.9 Hz, 4H), 7.43 – 7.40 (m, 1H), 7.23 (d, *J* = 8.2 Hz, 1H), 2.45 (s, 3H). ¹³C NMR (101 MHz, DMSO) δ 141.02, 139.91, 139.87, 136.32, 136.21, 135.42, 134.27, 134.19, 128.91, 127.60, 126.40, 126.27, 122.38, 122.27, 21.41. HRMS calcd for C₂₁H₆N₄Cl₂ [M+H]⁺, 395.0825; found, 395.0815

4.1.4.8 *N*²,*N*³-bis(4-bromophenyl)-6-methylquinoxaline-2,3-diamine (**6h**)

Yield 67%, light yellow solid. m.p.: 234-236 °C. ¹H NMR (500 MHz, DMSO-*d*₆) δ 9.49 (s, 2H), 7.97 (t, *J*=8.8 Hz, 4H), 7.58 (m, *J*=9.0, 3.0 Hz, 4H), 7.50 (d, *J*=8.3 Hz, 1H), 7.42 (s, 1H), 7.24 (d, *J*=8.3Hz, 1H), 2.45 (s, 3H). ¹³C NMR (101 MHz, DMSO-*d*₆) δ 141.49, 140.98, 140.30, 136.09, 135.47, 134.17, 131.80, 127.63, 125.46, 125.28, 122.80, 122.69, 114.40, 114.26, 21.41. HRMS calcd for C₂₁H₁₆Br₂N₄ [M+H]⁺, 482.9814; found: 482.9842

4.1.4.9 *N*²,*N*³-bis(3,4-dichlorophenyl)-6-methylquinoxaline-2,3-diamine (**6i**)

Yield 81%, light yellow solid. m.p.: 169-171 °C. ¹H NMR (500 MHz, DMSO-*d*₆) δ 9.22 (s, 1H), 9.19 (s, 1H), 8.32 (d, *J* = 2.5 Hz, 1H), 8.28 (d, *J* = 2.5 Hz, 1H), 7.86 (td, *J* = 8.3, 2.5 Hz, 2H), 7.65 (dd, *J* = 8.8, 3.2 Hz, 2H), 7.53 (d, *J* = 8.3 Hz, 1H), 7.47 – 7.43 (m, 1H), 7.29 (dd, *J* = 8.3,

2.0 Hz, 1H), 2.47 (s, 3H). ¹³C NMR (101 MHz, DMSO-*d*₆) δ 141.31, 141.07, 140.98, 140.75, 136.42, 136.16, 134.50, 131.26, 130.90, 128.26, 125.85, 125.63, 123.91, 123.77, 121.47, 121.35, 120.49, 120.36, 21.42. HRMS calcd for C₂₁H₁₄Cl₄N₄ [M+Na]⁺, 484.9973; found: 484.9858

4.1.4.10 6-methyl-*N*²,*N*³-di-*p*-tolylquinoxaline-2,3-diamine (**6j**)

Yield 80%, light yellow solid. m.p.: 161-163 °C. ¹H NMR (500 MHz, DMSO-*d*₆) δ 8.89 (s, 1H), 8.85 (s, 1H), 7.78 (dd, *J* = 10.4, 8.2 Hz, 4H), 7.43 (d, *J* = 8.2 Hz, 1H), 7.37 – 7.33 (m, 1H), 7.22 (dd, *J* = 8.4, 2.5 Hz, 4H), 7.20 – 7.14 (m, 1H), 2.43 (s, 3H), 2.34 (d, *J* = 2.9 Hz, 6H). ¹³C NMR (101 MHz, DMSO) δ 141.73, 141.22, 138.24, 138.17, 136.55, 134.75, 134.60, 131.95, 131.83, 129.51, 127.03, 125.44, 125.35, 121.16, 121.08, 21.40, 20.99. HRMS calcd for C₂₅H₂₆N₄ [M+H]⁺, 355.1917; found: 355.1926

4.1.4.11 *N*²,*N*³-bis(4-ethylphenyl)-6-methylquinoxaline-2,3-diamine (**6k**)

Yield 45%, yellow-green solid. m.p.: 155-158 °C. ¹H NMR (500 MHz, DMSO-*d*₆) δ 8.91 (s, 1H), 8.86 (s, 1H), 7.80 (t, *J* = 8.3 Hz, 4H), 7.43 (d, *J* = 8.2 Hz, 1H), 7.35 (s, 1H), 7.28 – 7.23 (m, 4H), 7.17 (d, *J* = 8.2 Hz, 1H), 2.64 (qd, *J* = 7.5, 2.5 Hz, 4H), 2.43 (s, 3H), 1.24 (t, *J* = 7.7 Hz, 6H). ¹³C NMR (101 MHz, DMSO) δ 141.09, 140.57, 138.20, 138.08, 137.01, 136.91, 135.53, 134.11, 133.59, 126.94, 125.72, 123.90, 123.79, 119.82, 27.16, 19.23, 14.18. HRMS calcd for C₂₅H₂₆N₄ [M+H]⁺, 383.2230; found, 383.2224.

4.1.4.12 6-methyl-*N*²,*N*³-bis(4-propylphenyl)quinoxaline-2,3-diamine (**6l**)

Yield 72%, light yellow solid. m.p.: 144-146 °C. ¹H NMR (500 MHz, DMSO-*d*₆) δ 8.91 (s, 1H), 8.87 (s, 1H), 7.81 (t, *J* = 8.3 Hz, 4H), 7.44 (d, *J* = 8.1 Hz, 1H), 7.39 – 7.35 (m, 1H), 7.23 (dd, *J* = 8.4, 3.2 Hz, 4H), 7.17 (dd, *J* = 8.3, 1.8 Hz, 1H), 2.62 – 2.55 (m, 3H), 2.43 (s, 3H), 1.64 (h, *J*

= 7.5 Hz, 4H), 0.95 (t, $J = 7.3$ Hz, 6H). ^{13}C NMR (101MHz, DMSO- d_6) δ 141.67, 141.15, 138.50, 138.41, 136.75, 136.56, 134.74, 134.62, 128.87, 127.03, 125.44, 125.36, 121.01, 120.89, 37.25, 24.69, 21.40, 14.15. HRMS calcd for $\text{C}_{27}\text{H}_{30}\text{N}_4$ $[\text{M}+\text{H}]^+$, 411.2543; found, 411.2537.

4.1.5 General Procedure for the synthesis of target compounds **7a-c**

According to the literature [15], a solution of 70% ethyl amine (2 equiv.) was dropwise added to a solution of compound **3a** (1 equiv.) dissolved in absolute ethanol (50 mL). The reaction mixture was then refluxed for 8 h. The solvent was evaporated under reduced pressure. The residue was purified by flash column chromatography with petroleum ether/ethyl acetate (10:1) as the eluent to afford 3-chloro-N-ethylquinoxalin-2-amine (**4**) as a white solid. The intermediate **4** was directly used for the next reaction. It was dissolved in DMF (50 mL), to which aromatic amine (1 equiv) and AlCl_3 (1.1 equiv.) were added. The mixture was stirred at 110°C for 8 h, then the reaction was quenched by cold water (50 mL). The product was extracted with ethyl acetate (3×75 mL), and the organic phase was washed with water (2×20 mL) and brine (30 mL), dried with anhydrous Na_2SO_4 . The solvent was evaporated under reduced pressure and the solid was purified by flash column chromatography with petroleum ether/ethyl acetate (10:1) as the eluent

4.1.5.1 N^2 -ethyl- N^3 -(4-fluorophenyl)quinoxaline-2,3-diamine (**7a**)

Yield 59%, yellow solid. m.p.: $138\text{--}140^\circ\text{C}$. ^1H NMR (500 MHz, DMSO- d_6) δ 8.77 (s, 1H), 7.94 (dd, $J = 9.0, 5.0$ Hz, 2H), 7.50 (d, $J = 7.9$ Hz, 2H), 7.30 (t, $J = 7.5$ Hz, 1H), 7.27 – 7.21 (m, 3H), 7.18 (d, $J = 5.0$ Hz, 1H), 3.58 (qd, $J = 7.3, 4.7$ Hz, 2H), 1.34 (t, $J = 7.2$ Hz, 3H). ^{13}C NMR (101 MHz, DMSO- d_6) ^{13}C NMR (101 MHz, DMSO) δ 144.19, 141.04, 137.85, 137.14,

137.11, 135.54, 125.74, 125.29, 125.18, 124.02, 122.42, 122.34, 115.73, 115.51, 36.37, 14.67.

HRMS calcd for C₁₆H₁₅N₄F [M-H]⁻, 281.1194; found, 281.1208

4.1.5.2 N²-ethyl-N³-(4-chlorophenyl)quinoxaline-2,3-diamine (**7b**)

Yield 78%, light yellow solid. m.p.: 142-144 °C. ¹H NMR (500 MHz, DMSO-*d*₆) δ 8.84 (s, 1H), 7.98 (d, *J* = 8.7 Hz, 2H), 7.52 (dd, *J* = 13.0, 8.0 Hz, 2H), 7.45 (d, *J* = 8.6 Hz, 2H), 7.32 (t, *J* = 7.4 Hz, 1H), 7.26 (t, *J* = 7.5 Hz, 1H), 7.21 (t, *J* = 4.9 Hz, 1H), 3.58 (qd, *J* = 7.4, 4.9 Hz, 2H), 1.33 (t, *J* = 7.3 Hz, 3H). ¹³C NMR (101 MHz, DMSO-*d*₆) δ 144.27, 140.77, 139.84, 138.0, 135.4, 128.9, 126.2, 125.87, 125.57, 125.24, 124.07, 121.98, 36.38, 14.67. HRMS calcd for C₁₆H₁₅N₄Cl₄ [M-H]⁻, 297.0912; found, 297.0911

4.1.5.3 N²-ethyl-N³-(4-bromophenyl)quinoxaline-2,3-diamine (**7c**)

Yield 77%, light yellow solid. m.p.: 150-153 °C. ¹H NMR (500 MHz, DMSO-*d*₆) δ 8.84 (s, 1H), 7.98 (d, *J* = 8.6 Hz, 2H), 7.52 (dd, *J* = 13.0, 7.9 Hz, 2H), 7.45 (d, *J* = 8.6 Hz, 2H), 7.32 (t, *J* = 7.4 Hz, 1H), 7.26 (t, *J* = 7.4 Hz, 1H), 7.21 (t, *J* = 4.9 Hz, 1H), 3.58 (qd, *J* = 7.4, 5.0 Hz, 2H), 1.33 (t, *J* = 7.2 Hz, 3H). ¹³C NMR (101 MHz, DMSO-*d*₆) δ 144.29, 140.73, 140.26, 137.96, 135.37, 131.83, 125.89, 125.61, 125.24, 124.08, 122.39, 114.12, 36.38, 14.66. HRMS calcd for C₁₆H₁₅BrN₄ [M+H]⁺, 343.0553; found, 343.0541

4.1.6 General Procedure for the synthesis of target compounds **8a-c**

The synthesis of **8a-c** was almost the same as that of **7a-c**, except for a solution of chlorobenzenesulfonamide was used to react with compound **3a**.

4.1.6.1 4-chloro-N-(3-((4-fluorophenyl)amino)quinoxalin-2-yl)benzenesulfonamide (**8a**)

Yield 61%, light yellow solid. m.p.: 244-247 °C. ¹H NMR (500 MHz, DMSO-*d*₆) δ 12.36 (s, 1H), 9.10 (s, 1H), 8.16 (d, *J* = 8.3 Hz, 2H), 8.06 – 7.98 (m, 2H), 7.97-7.84 (m, 1H), 7.70 (d, *J* =

8.4 Hz, 2H), 7.56 (d, $J = 7.7$ Hz, 1H), 7.39 (p, $J = 7.1$ Hz, 2H), 7.23 (t, $J = 8.8$ Hz, 2H). ^{13}C NMR (101 MHz, DMSO) δ 159.83, 157.41, 137.86, 135.80, 135.76, 135.72, 129.56, 128.83, 126.55, 126.04, 125.94, 123.32, 115.69, 115.47. HRMS calcd for $\text{C}_{20}\text{H}_{14}\text{ClFN}_4\text{O}_2\text{S}$ $[\text{M}+\text{H}]^+$, 428.0499; found, 428.0483

4.1.6.2 4-chloro-N-(3-((3,4-difluorophenyl)amino)quinoxalin-2-yl)benzenesulfonamide (8b)

Yield 73%, yellow-green solid. m.p.: 253–255 °C. ^1H NMR (500 MHz, DMSO- d_6) δ 12.37 (s, 1H), 9.23 (s, 1H), 8.31 – 8.21 (m, 1H), 8.16 – 8.10 (m, 2H), 7.94 – 7.89 (m, 1H), 7.85 – 7.77 (m, 1H), 7.71 – 7.64 (m, 2H), 7.63 – 7.55 (m, 1H), 7.47 – 7.39 (m, 1H), 7.42 – 7.34 (m, 2H). ^{13}C NMR (126 MHz, DMSO) δ 150.25, 150.15, 148.33, 148.22, 146.66, 144.64, 141.61, 140.57, 137.85, 136.53, 129.54, 128.91, 126.56, 126.33, 126.21, 117.62, 117.48, 110.02. HRMS calcd for $\text{C}_{20}\text{H}_{13}\text{N}_4\text{O}_2\text{F}_2\text{S}$ $[\text{M}+\text{H}]^+$, 447.0489; found:447.0487.

4.1.6.3 4-chloro-N-(3-(p-tolylamino)quinoxalin-2-yl)benzenesulfonamide (8c)

Yield 70%, light yellow solid. m.p.: 226–228 °C. ^1H NMR (500 MHz, DMSO- d_6) δ 12.33 (s, 1H), 8.93 (s, 1H), 8.15 (d, $J = 8.3$ Hz, 2H), 7.96–7.88 (m, 1H), 7.85 (d, $J = 8.0$ Hz, 2H), 7.69 (d, $J = 8.3$ Hz, 2H), 7.56 (d, $J = 7.8$ Hz, 1H), 7.40 (t, $J = 7.4$ Hz, 1H), 7.36 (t, $J = 7.5$ Hz, 1H), 7.20 (d, $J = 8.1$ Hz, 2H), 2.32 (s, 3H). ^{13}C NMR (101 MHz, DMSO) δ 141.71, 140.65, 137.83, 136.76, 132.86, 129.56, 129.51, 128.96, 126.53, 126.01, 125.76, 121.19, 114.20, 109.80, 20.99. HRMS calcd for $\text{C}_{21}\text{H}_{17}\text{N}_4\text{O}_2\text{S}\text{Cl}$ $[\text{M}+\text{Na}]^+$, 447.0653; found, 447.0656.

4.2 Computational Modeling

4.2.1 Pharmacophore model generation

The Catalyst/HipHop implemented in Discovery Studio was used to generate common

feature pharmacophores based on the ligands in the modeling set. The ligands were prepared by using the “prepare ligand” module. This module added hydrogen atoms to the chemical structures and generated the protonated state at the pH of 7.4. The “Principal” and “MaxOmitFeat” properties were assigned to the ligands according to their MIC values for *S. aureus* ATCC29213. To be specific, the values of 2 and 0 were respectively assigned to the “Principal” and the ‘MaxOmitFeat’ attributes of **6a-d**, which indicated that these compounds were highly active and none of the pharmacophore features from them were allowed to omit in model generation. For the other two moderately active compounds, i.e. **6e** and **6f**, both the “Principal” and the “MaxOmitFeat” attributes were set as 1. The “Fast” method was applied to quickly generate a maximum of 255 diverse low-energy conformations of each ligand, within the relative energy threshold of 20 kcal/mol. The “Feature Mapping” module was applied to identify possible locations of different pharmacophore features in the generated ligand conformations. From 272 features, hydrogen bond acceptor, hydrogen bond donor, general hydrophobic features including those from aromatic rings and from aliphatic chains, ring aromatic features were the most frequent and important features. In the module of “Common Feature Pharmacophore Generation”, the above-mentioned features were selected and the allowed number of each feature in a pharmacophore was set as 0 to 5. A maximum of 10 models were allowed to generate by this module.

The pharmacophore models were evaluated with a data set composed of 12 newly-synthesized active/inactive compounds. The “Ligand Profiler” module in Discovery Studio was run to map all the compounds to every generated pharmacophore model. In the module, the parameter of “Maximum Omitted Features” was set to -1, indicating all feature

subsets of the pharmacophore were considered in model evaluation. Other parameters were set as default. The pharmacophore model that can best discriminate actives from inactives by FitValue was regarded as the optimal model.

4.2.2 Shape generation

The lowest-energy conformation of the most active derivative **6c** was generated by the “Quick Minimization” tool in Discovery Studio. Based on the conformation, ROCS (version 3.3.1.2, OpenEye Scientific Software Inc., Santa Fe, NM, USA) was used to generate the shape-based model. During the shape generation, no additional editing of the model was performed.

4.2.3 Virtual screening

The Specs chemical library that included more than 210,000 compounds (version Jun. 2019, accessed at <http://www.specs.net>) was used for the virtual screening. The compounds in the library were prepared by the “Prepare Ligands” module in DS. The ligand preparation included the generation of all protonated states at the pH of 7.4 and the enumeration of all potential stereoisomers. A multi-conformer database of the prepared structures was built by the “Build 3D Database” module in Discovery Studio. In the database, each prepared structure is represented by a maximum of 100 conformers. As the first step, all the conformers in the 3D database were mapped to the pharmacophore model (i.e. Pharm_07) by a rigid fit algorithm (“FAST” search) implemented in the “Search 3D Database” module in DS. The similarity of pharmacophore features was measured by the metric of FitValue. All the conformers with the FitValues greater than zero were put out. For the conformers/stereoisomers that belong to the same Specs IDNUMBER, only the

conformer/stereoisomer that best matched the pharmacophore model was saved. Then, a certain number of compounds that passed the pharmacophore filter were mapped to the shape-based model by ROCS. ShapeTanimoto was the scoring function to measure shape similarity. Subsequently, the “Find Similar Molecules by Fingerprints” module in DS was used for 2D similarity search. In this module, the most active derivative **6c** in the modeling set was set as the reference. FCFP-6 was the molecular fingerprinting algorithm and Tc was the metric to measure similarity. In order to identify diverse hits, only the compounds with the Tc value less than 0.3 were retained. Structural clustering based on FCFP-6 fingerprints was performed to generate 25 clusters, from which the potential hits were selected by taking pharmacophore FitValue, shape Tc and fingerprints Tc as well as synthetic feasibility, commercial availability into consideration.

4.2.4 Molecular Docking

The X-ray structure of *S. aureus* GyrB in complex with novobiocin (PDB code: 4URO) was downloaded from the Protein Data Bank (<https://www.rcsb.org>). Then, the identical protein chains and the cocrystallized water molecules were deleted, and the cognate ligand (novobiocin) was stripped from the crystal structure and saved for future use. The “Clean Protein” tool of Discovery Studio was used to solve potential problems in the protein structure such as nonstandard names, incomplete residues, nonstandard atom orders, alternate conformations, as well as incorrect connectivity and bond orders, modify all hydrogen atoms and terminal residues, and generate the protonation state at pH 7.0.

As the first step of molecular docking using OpenEye (OpenEye Scientific Software, Inc., Santa Fe, NM, USA), a maximum of 200 conformers was generated by the module named

OMEGA (version 2.5.1.4) [25]. Secondly, the prepared protein structure was converted to a receptor by OEDocking (version 3.0.1) [26], with the cognate ligand to define the binding site. Thirdly, all the conformers of the compound were positioned in the binding site of the receptor and scored by the Chemgauss4 scoring function in OEDocking. Lastly, the top-scoring pose was retained and used as the initial binding mode between the compound and GyrB.

4.2.5 Molecular dynamics simulation

The all-atom MD simulation was performed for every GyrB-ligand complex with AMBER 20 software [27] on GPUs. The initial structure of the complex was generated by the above-mentioned molecular docking. Each system was composed of a GyrB protein, a ligand, around 10,700 TIP3P water molecules, and 8 Na⁺ ions that neutralize the whole system. The partial atomic charges of the ligand were the AM1-BCC charges calculated by the *antechamber* module of the AMBER software package, while the other force field parameters of the ligand were from GAFF2. The AMBER FF14SB force field was applied to the GyrB protein. *Antechamber* and *LEaP* were used to generate the topology files of ligands and GyrB, respectively.

For each protein-ligand complex, the solvent of the system was minimized by both the steepest descent method (5000 steps) and the conjugated gradient algorithm (20,000 steps). All the solute were restrained using a harmonic potential, with a force constant of 500 (kcal/mol)/Å². Each MD simulation consisted of the relaxation phase, the equilibrium phase, and the sampling phase. At the relaxation phase, the system was heated gradually from 0 K to 300 K, with a 5-ps simulation for each 50-K increase in temperature and a force constant of 2

(kcal/mol)/Å². At the temperature of 300 K, the system was simulated for 500 ps. At the equilibrium phase, the system was simulated at 1 bar for 10 ns, including 5-ns simulation with restraints and 5-ns simulation without any restraint. Lastly, a 100-ns MD simulation was performed for each system with no restraint. A total of 10 000 snapshots were recorded at this sampling phase. During the simulation, the temperature was regulated by the weak-coupling algorithm and the pressure was regulated by the isotropic position scaling algorithm with a pressure relaxation time of 1.0 ps. The integration of the equations of motion was conducted at a time interval of 0.5 fs at the heating phase and 2 fs for the other phases. All bonds were constrained using the SHAKE algorithm. The particle-mesh Ewald (PME) method was used to calculate long-range electrostatic interactions.

4.3 Biology

4.3.1 Bacterial growth inhibition assay

The broth microdilution assay recommended by the Clinical and Laboratory Standards Institute [13] was performed to determine the MICs of the compounds. The 2-fold dilutions of the compound dissolved in MH broth medium/DMSO (100 µL) were added to 12 wells of the 96-well plate, followed by the addition of the bacterial suspension (100 µL) to each well. The resulting solutions of the compound were at the concentrations from 100 to 0.05 µg/mL (for *S. aureus* ATCC29213) or 64 to 0.03 µg/mL (for MRSA), while the resulting concentration of the bacterial suspension was approximately 10⁵ CFU/ml. After incubation at 37 °C for 18–24 h, the MIC value was determined by visual inspection. The MIC was the lowest concentration at which the bacterial growth was completely inhibited. The assay was performed in duplicate.

4.3.2 *S. aureus* GyrB inhibition assay

The reaction mixture of the assay (10 μ L) includes 5 nM *S. aureus* Gyrase (Inspiralis Ltd., Norwich, United Kingdom), the buffer (40 mM HEPES-KOH (pH 7.6), 10 mM magnesium acetate, 10 mM dithiothreitol, 50 g/L BSA, 500 mM potassium glutamate), the compound at the test concentration, 1% DMSO, 10 nM linear pBR322 DNA, 100 mM ATP. Firstly, the solutions of the compound at 10 times the test concentration were prepared by using the assay buffer and DMSO as solvents. Then, the compound solution (1 μ L) was put into a PCR tube, followed by the sequential adding of the buffer (7 μ L), the linear pBR322 DNA (0.5 μ L) and *S. aureus* Gyrase (0.5 μ L) as well as the ATP (1 μ L). The reaction mixture was incubated at 37 °C for 30 min.

To quantify the generated ADP, ADP-Glo kits were used. The ADP-Glo reagent (40 μ L) was added to the mixture and incubated at 37 °C for 40 min. Following that, the detection reagent (50 μ L) was added and the mixture was incubated at another 5 min. The luminescence of the mixture was recorded by the BioTek Synergy 2 microplate reader. The enzymatic activity (%) after compound treatment at the test concentration was calculated based on the luminescence of the mixtures with the compound and without the compound. According to the activity values (%) of the enzyme after the treatment with different concentrations of the compound (i.e. 0.01 μ M -100 μ M), the IC₅₀ value was determined by using GraphPad Prism 5 software (GraphPad Software Inc., La Jolla, CA). The compounds were tested in duplicate. Novobiocin was the positive control of this assay.

4.2.2. Cytotoxicity assay

The SRB assay was used to determine the cytotoxicity. The cells (HepG2 or HUVEC)

seeded in 96-well plates were treated with the 3-fold dilutions of the compounds (i.e. 0.01 μ M-100 μ M), and incubated at the conditions of 37 °C and 5% CO₂ for 72 h. Then, the cells were fixed with 10 % trichloroacetic acid (w/v), kept at 4 °C for 1 h, and washed with distilled water for 5 times and air-dried. Next, the cells were stained with 0.4% (w/v) sulforhodamine B (SRB) at the room temperature for 20 min and washed with 1% acetic acid for 5 times. Lastly, the bound SRB was solubilized with 10 mM Tris and the absorbance in term of optical density was measured at 540 nm by using a Tecan Infinite M1000 microplate reader. According to the cell viability (%) after the treatment with different concentrations of the compounds, the CC₅₀ value was determined by using GraphPad Prism 5 software (GraphPad Software Inc., La Jolla, CA). Paclitaxel was used as the positive drug for this assay. The assay was performed in duplicate.

ASSOCIATED CONTENT

AUTHOR INFORMATION

Corresponding Author

*E-mail: J.X. (jie.william.xia@hotmail.com) and S.W. (ws@imm.ac.cn)

Address: Jie Xia & Song Wu, Department of New Drug Research and Development, Institute of Materia Medica, Chinese Academy of Medical Sciences and Peking Union Medical College, Beijing 100050, China

Declaration of competing interest

The authors declare no competing financial interest.

Author Contributions

J.X. conceived and supervised the project. J.X. designed the experiments. X.L, Z.X., P. K.,

H.J. and I. T. contributed to the computational modeling. X. L. and X.L performed chemical synthesis and bioassays. J.X, X. L. and Z.X contributed to the writing of the manuscript. J.X. and S.W. assume responsibility for the manuscript in its entirety.

ORCID

Xu Lian: 0000-0002-7599-317X

Zhonghua Xia: 0000-0002-4219-374X

Xueyao Li: 0000-0001-8739-3801

Pavel Karpov: 0000-0003-4786-9806

Igor V. Tetko: 0000-0002-6855-0012

Jie Xia: 0000-0002-9567-3763

Song Wu: 0000-0001-7876-7007

Acknowledgments

This work was supported by the CAMS Innovation Fund for Medical Sciences (Grant No. 2017-I2M-1-012) and PUMC Graduate Students Innovation Fund (Grant No. 2019-1007-01) and by the China Scholarship Council (CSC) for Z.X. (Grant No. 201706880010). We are grateful to Sichuan Primed Bio-Tech Group Co., Ltd for the bioassays against MRSA. We also thank Dr. Wenxuan Zhang and Dr. Tianlei Li for helpful discussions on the chemical synthesis.

Appendix A. Supplementary data

Supplementary data related to this article can be found at xxx.

Abbreviations

MRSA, methicillin-resistant *S. aureus*; GyrB, Gyrase B; WHO, World Health Organization;

MSSA, methicillin-sensitive *S. aureus*; Tc, Tanimoto coefficient; MD, molecular dynamics; sulforhodamine B, SRB; HepG2, hepatocellular carcinoma; HUVEC, human umbilical vein endothelial cells; TLC, thin layer chromatography; HRMS, high resolution mass spectrometry.

References

- [1] J.M. Stokes, K. Yang, K. Swanson, W. Jin, A. Cubillos-Ruiz, N.M. Donghia, C.R. MacNair, S. French, L.A. Carfrae, Z. Bloom-Ackermann, V.M. Tran, A. Chiappino-Pepe, A.H. Badran, I.W. Andrews, E.J. Chory, G.M. Church, E.D. Brown, T.S. Jaakkola, R. Barzilay, J.J. Collins, A Deep Learning Approach to Antibiotic Discovery, *Cell* 180(4) (2020) 688-702 e13.
- [2] L.B. Rice, Federal funding for the study of antimicrobial resistance in nosocomial pathogens: no ESKAPE, *J. Infect. Dis.* 197(8) (2008) 1079-81.
- [3] E. Tacconelli, E. Carrara, A. Savoldi, S. Harbarth, M. Mendelson, D.L. Monnet, C. Pulcini, G. Kahlmeter, J. Kluytmans, Y. Carmeli, M. Ouellette, K. Outtersson, J. Patel, M. Cavaleri, E.M. Cox, C.R. Houchens, M.L. Grayson, P. Hansen, N. Singh, U. Theuretzbacher, N. Magrini, W.H.O.P.P.L.W. Group, Discovery, research, and development of new antibiotics: the WHO priority list of antibiotic-resistant bacteria and tuberculosis, *Lancet Infect. Dis.* 18(3) (2018) 318-327.
- [4] M. Bassetti, A. Russo, A. Carnelutti, M. Wilcox, Emerging drugs for treating methicillin-resistant *Staphylococcus aureus*, *Expert Opin. Emerging Drugs* 24(3) (2019) 191-204.

- [5] P. Fernandes, E. Martens, Antibiotics in late clinical development, *Biochem. Pharmacol.* 133 (2017) 152-163.
- [6] W.P. Walters, R. Wang, New Trends in Virtual Screening, *J. Chem. Inf. Model.* 59(9) (2019) 3603-3604.
- [7] R.C. Diniz, L.W. Soares, L.C. Nascimento da Silva, Virtual Screening for the Development of New Effective Compounds Against *Staphylococcus aureus*, *Curr. Med. Chem.* 25(42) (2018) 5975-5985.
- [8] I.V. Semenyuta, M.M. Trush, V.V. Kovalishyn, S.P. Rogalsky, D.M. Hodyna, P. Karpov, Z. Xia, I.V. Tetko, L.O. Metelytsia, Structure-Activity Relationship Modeling and Experimental Validation of the Imidazolium and Pyridinium Based Ionic Liquids as Potential Antibacterials of MDR *Acinetobacter Baumannii* and *Staphylococcus Aureus*, *Int. J. Mol. Sci.* 22(2) (2021).
- [9] S. Hinsberger, K. Husecken, M. Groh, M. Negri, J. Haupenthal, R.W. Hartmann, Discovery of novel bacterial RNA polymerase inhibitors: pharmacophore-based virtual screening and hit optimization, *J. Med. Chem.* 56(21) (2013) 8332-8.
- [10] E. Karhu, J. Isojarvi, P. Vuorela, L. Hanski, A. Fallarero, Identification of Privileged Antichlamydial Natural Products by a Ligand-Based Strategy, *J. Nat. Prod.* 80(10) (2017) 2602-2608.
- [11] K. Mitra, A. Chadha, M. Doble, Pharmacophore based approach to screen and evaluate novel *Mycobacterium* cell division inhibitors targeting FtsZ - A modelling and experimental study, *Eur. J. Pharm. Sci.* 135 (2019) 103-112.

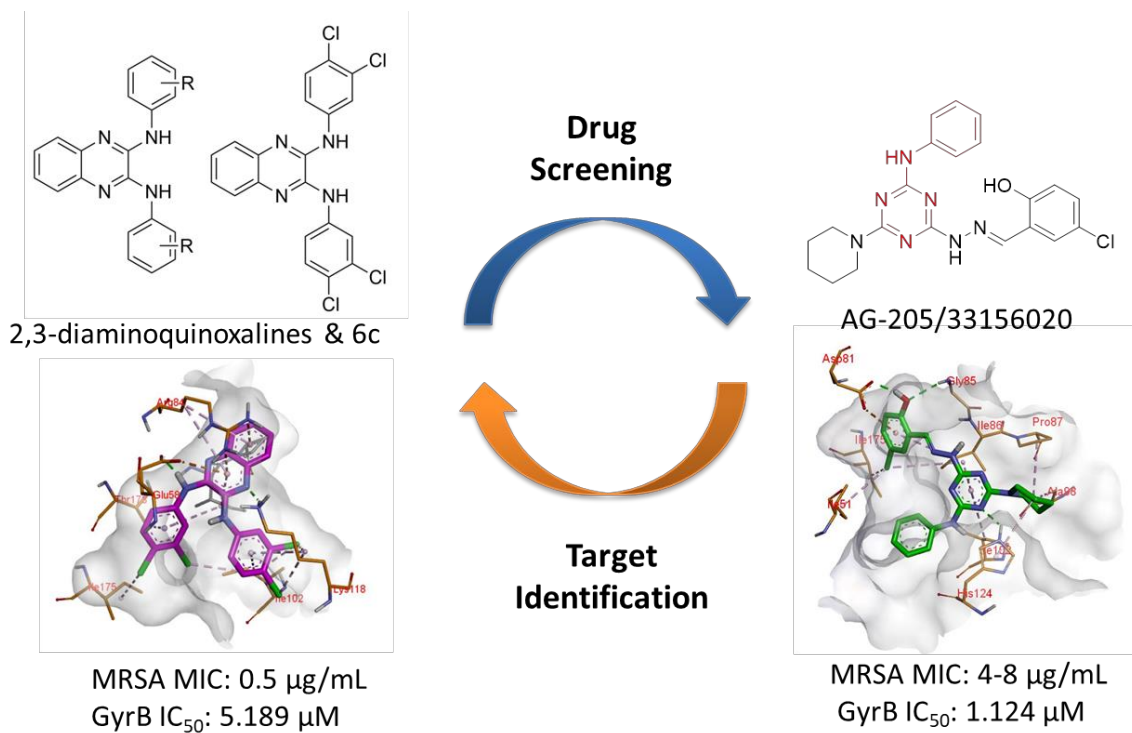
- [12] M.A. El-Atawy, E.A. Hamed, M. Alhadi, A.Z. Omar, Synthesis and Antimicrobial Activity of Some New Substituted Quinoxalines, *Molecules* 24(22) (2019).
- [13] M.A. Wikler, Methods for dilution antimicrobial susceptibility tests for bacteria that grow aerobically : approved standard, CLSI (NCCLS) 26 (2006) M7-A7.
- [14] S.A.M. Khan, P.; Manchanda, H., Synthesis and antimicrobial activity of 2,3-di-substituted quinoxalines, *Indian J. Heterocycl. Chem.* 18(2) (2008) 197-198.
- [15] A. Keivanloo, M. Bakherad, A. Rahimi, Synthesis of Unexpected Pyrrolo[2,3-b]quinoxaline-2-carbaldehydes via Sonogashira Coupling Reaction, *Synthesis* 2010(10) (2010) 1599-1602.
- [16] S.V. Litvinenko, V.I. Savich, L.D. Bobrovnik, Synthesis, structure, and chemical properties of some N-(3-chloro-2-quinoxaly)arylsulfonamides, *Chem. Heterocycl. Compd.* 30(3) (1994) 340-344.
- [17] K. Ingram-Sieber, N. Cowan, G. Panic, M. Vargas, N.R. Mansour, Q.D. Bickle, T.N. Wells, T. Spangenberg, J. Keiser, Orally active antischistosomal early leads identified from the open access malaria box, *PLoS Negl Trop Dis* 8(1) (2014) e2610.
- [18] B.T. J.P. Poyser, D. Timms, M.H. Block, N.J. Hales, Triazine derivatives and their use as antibacterials, *WO Pat* (1999), 99/01442.
- [19] Z. Jakopin, J. Ilas, M. Barancokova, M. Brvar, P. Tammela, M. Sollner Dolenc, T. Tomasic, D. Kikelj, Discovery of substituted oxadiazoles as a novel scaffold for DNA gyrase inhibitors, *Eur. J. Med. Chem.* 130 (2017) 171-184.

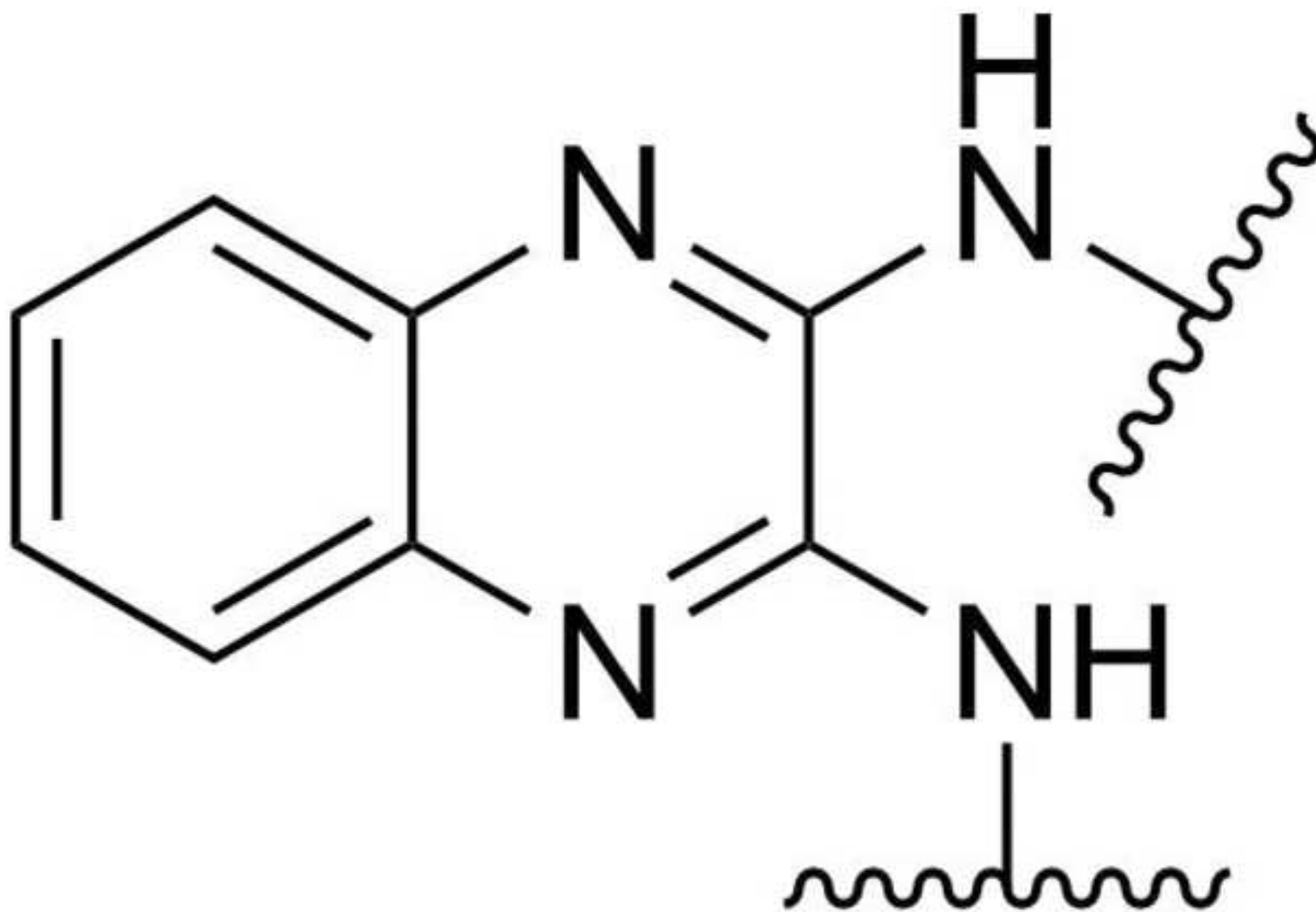
- [20] N.S. Haiba, H.H. Khalil, M.A. Moniem, M.H. El-Wakil, A.A. Bekhit, S.N. Khattab, Design, synthesis and molecular modeling studies of new series of s-triazine derivatives as antimicrobial agents against multi-drug resistant clinical isolates, *Bioorg. Chem.* 89 (2019) 103013.
- [21] D.R. Roe, T.E. Cheatham, PTRAJ and CPPTRAJ: Software for Processing and Analysis of Molecular Dynamics Trajectory Data, *J. Chem. Theory Comput.* 9(7) (2013) 3084-3095.
- [22] H. Quan, H. Liu, C. Li, L. Lou, 1,4-Diamino-2,3-dicyano-1,4-bis(methylthio)butadiene (U0126) Enhances the Cytotoxicity of Combretastatin A4 Independently of Mitogen-Activated Protein Kinase Kinase, *J. Pharmacol. Exp. Ther.* 330(1) (2009) 326.
- [23] G.S. Bisacchi, J.I. Manchester, A New-Class Antibacterial-Almost. Lessons in Drug Discovery and Development: A Critical Analysis of More than 50 Years of Effort toward ATPase Inhibitors of DNA Gyrase and Topoisomerase IV, *ACS Infect. Dis.* 1(1) (2015) 4-41.
- [24] J. Araújo, F.G. Menezes, H.F.O. Silva, D.S. Vieira, S.R.B. Silva, A.J. Bortoluzzi, C. Sant'Anna, M. Eugenio, J.M. Neri, L.H.S. Gasparotto, Functionalization of gold nanoparticles with two aminoalcohol-based quinoxaline derivatives for targeting phosphoinositide 3-kinases (PI3K α), *New J. Chem.* 43(4) (2019) 1803-1811.
- [25] P.C. Hawkins, A.G. Skillman, G.L. Warren, B.A. Ellingson, M.T. Stahl, Conformer generation with OMEGA: algorithm and validation using high quality structures from the Protein Databank and Cambridge Structural Database, *J. Chem. Inf. Model.* 50(4) (2010) 572-84.

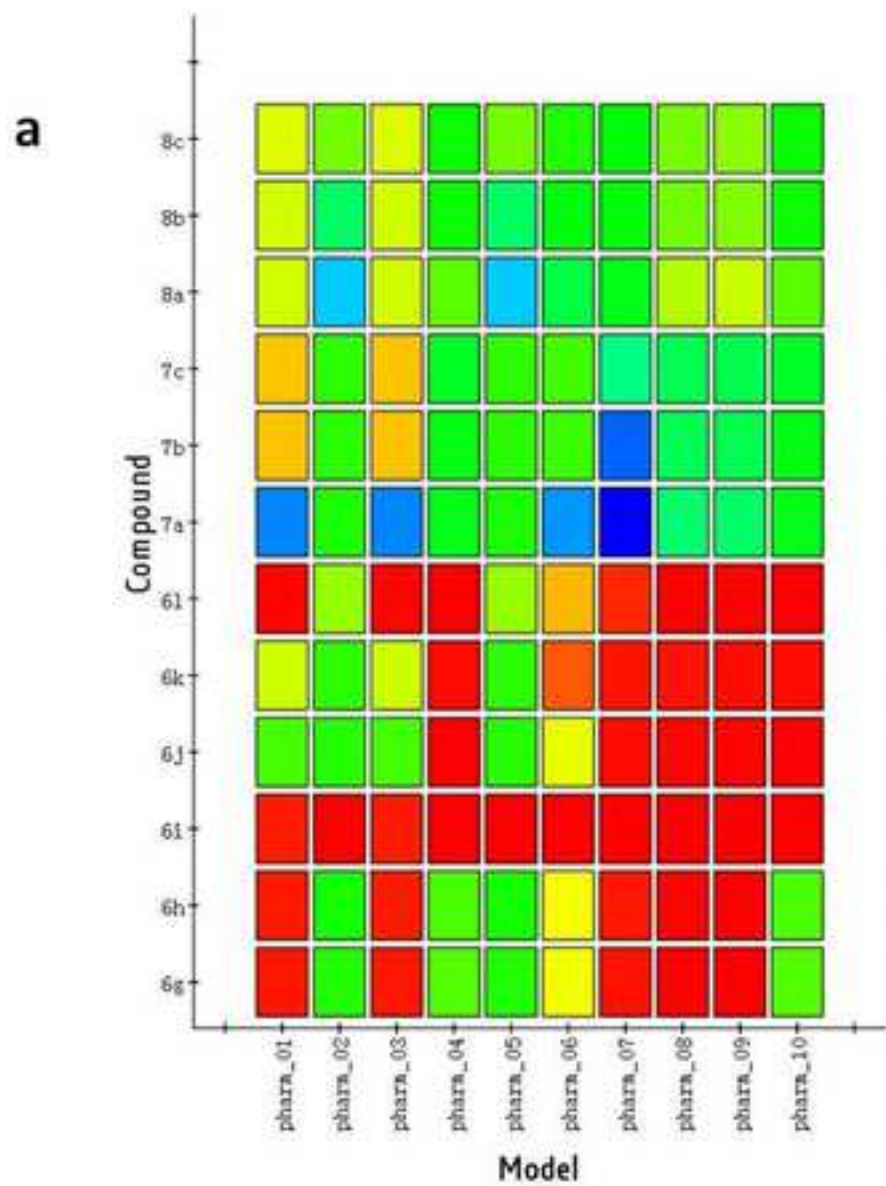
[26] M. McGann, FRED pose prediction and virtual screening accuracy, *J. Chem. Inf. Model.* 51(3) (2011) 578-96.

[27] K.B. D.A. Case, I.Y. Ben-Shalom, S.R. Brozell, D.S. Cerutti, T.E. Cheatham, III, V.W.D. Cruzeiro, T.A. Darden, R.E. Duke, G. Giambasu, M.K. Gilson, H. Gohlke, A.W. Goetz, R. Harris, S. Izadi, S.A. Izmailov, K. Kasavajhala, A. Kovalenko, R. Krasny, T. Kurtzman, T.S. Lee, S. LeGrand, P. Li, C. Lin, J. Liu, T. Luchko, R. Luo, V. Man, K.M. Merz, Y. Miao, O. Mikhailovskii, G. Monard, H. Nguyen, A. Onufriev, F. Pan, S. Pantano, R. Qi, D.R. Roe, A. Roitberg, C. Sagui, S. Schott-Verdugo, J. Shen, C.L. Simmerling, N.R. Skrynnikov, J. Smith, J. Swails, R.C. Walker, J. Wang, L. Wilson, R.M. Wolf, X. Wu, Y. Xiong, Y. Xue, D.M. York and P.A. Kollman (2020), AMBER 2020, University of California, San Francisco.

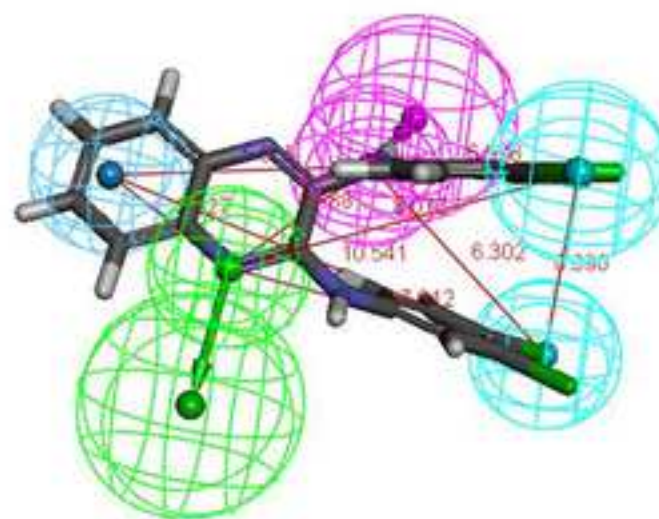
Table of Contents Graphic







b



c

